HHS Public Access

Author manuscript

Biochemistry. Author manuscript; available in PMC 2018 August 15.

Published in final edited form as:

Biochemistry. 2017 August 15; 56(32): 4244–4255. doi:10.1021/acs.biochem.7b00348.

Specific Histidine Residues Confer Histatin Peptides with Copper-Dependent Activity against *Candida albicans*

Steven E. Conklin[a], **Emma C. Bridgman**[b], **Qiang Su**[a], **Pamela Riggs-Gelasco**[c], **Kathryn L. Haas**[b], and **Katherine J. Franz**[a,*]

[a]Department of Chemistry, Duke University, Durham, North Carolina, USA

[b]Department of Chemistry & Physics, Saint Mary's College, Notre Dame, Indiana, USA

[c]Department of Chemistry and Biochemistry, College of Charleston, Charleston, South Carolina, USA

Abstract

The histidine-rich salivary peptides of the histatin family are known to bind copper (Cu) and other metal ions in vitro, but the details of these interactions are poorly understood and their implications on in vivo antifungal activity have not been established. Here, we show that availability of Cu during exposure of *Candida albicans* to histatin-5 (Hist-5) modulates its antifungal activity. Antifungal susceptibility testing revealed that co-treatment of Hist-5 with Cu improved the EC_{50} from ~5 μM to ~1 μM, whereas co-treatment with a high-affinity Cu-specific chelator abrogated antifungal activity. Spectrophotometric titrations revealed two previously unrecognized Cu(I) binding sites with apparent K_d values at pH 7.4 ~ 20 nM, and confirmed a high-affinity Cu(II) binding site at the Hist-5 N-terminus with apparent K_d ~ 8 pM. Evaluation of a series of His-to-Ala peptides containing the first 12 residues of Hist-5 identified adjacent His residues (*bis*-His) as critical anchors for Cu(I) binding, and the presence of a third ligand was revealed by X-ray absorption spectroscopy (XAS). On their own, the truncated peptides were ineffective at inhibiting growth of *C. albicans*, but treatment with supplemental Cu resulted in EC_{50} values down to ~ 5 μM, approaching that of full-length Hist-5. The efficacy of the peptides depended on an intact *bis*-His site and correlated with Cu(I) affinity. Together, these results establish new structure-function relationships linking specific histidine residues with Cu-binding affinity and antifungal activity, and provide further evidence for the involvement of metals in modulating the biological activity of these antifungal peptides.

SYNOPSIS TOC

*Corresponding Author. Katherine J. Franz, katherine.franz@duke.edu.

ASSOCIATED CONTENT

Supporting Information

Additional spectrophotometric assays, table of XAS structural results, antifungal susceptibility assays, and equations used for calculation of apparent binding constants. The Supporting Information is available free of charge on the ACS Publications website.

The authors declare no competing financial interests.

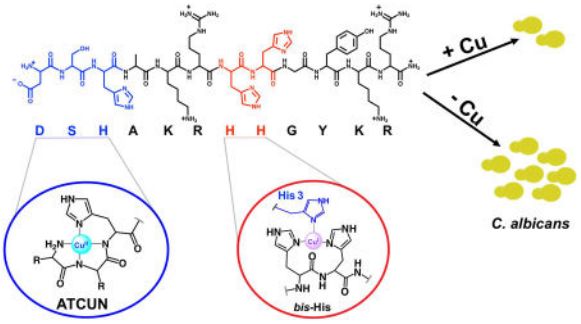

Spectroscopic titrations, XAS and antifungal assays were used to explore the relationship between copper-binding and antifungal properties of the salivary peptide Histatin-5. Copper availability was shown to modulate the cytotoxicity of Hist-5 against *Candida albicans*, and evidence suggests that such modulation is due to a direct interaction between Cu and the peptide. Adjacent His residues (*bis*-His) were identified to be critical for Cu(I) binding, and that the efficacy of the peptide depends on an intact *bis*-His site. Therefore, our results provide evidence suggesting that the *bis*-His site may not only serve as a primary anchor for Cu(I) binding, but, once bound to Cu(I), may also be responsible for the antifungal activity of Hist-5. Together, these results establish new structure-function relationships linking specific histidine residues with Cu-binding affinity and antifungal activity, and provide further evidence for the involvement of metals in modulating the biological activity of these antifungal peptides.

Keywords

Histatin; Cu(I); Cu(II); EXAFS; antifungal; peptide; metallopeptide; bis-His; ATCUN; Candida albicans

Human saliva contains numerous antimicrobial peptides that protect against bacterial, fungal and viral infection.[1] Among these are histatins, a family of twelve histidine-rich cationic peptides that range from 7 to 38 residues in length, and are weakly amphipathic. With a concentration of 15–30 μM, Histatin-5 (Hist-5) is the most abundant in saliva as well as the most effective at killing *Candida albicans* (median lethal dose ~ 2–10 μM), an opportunistic fungal pathogen commonly found in mucosal membranes.[2–5] While other classes of cationic antimicrobial peptides target the plasma membrane and kill by inducing pores, Hist-5's intrinsic disorder and lack of helicity in aqueous solution suggests that it operates by an alternative mechanism.[6–7] The mechanism of Hist-5 antimicrobial activity has been vigorously debated; however there is now general consensus that Hist-5's antimicrobial activity involves intracellular targets.[8–10] The evolution of understanding of Hist-5 candidacidal mechanism has been reviewed recently.[11]

Heat shock proteins Ssa1 and Ssa2 have been identified as the cell envelope binding proteins that facilitate Hist-5 cellular entry in *Candida*,[12] after which it has been shown to localize to the mitochondria and cause inhibition of the respiratory chain and propagation of reactive oxygen species (ROS).[13] While ROS have been implicated in fungal cell death,[14] the source and mechanism remain unclear.

ROS formation is commonly associated with redox-active metals, which has made the investigation of Hist-5's metal-binding properties an area of interest and speculation.[15] Indeed, Hist-5 possesses multiple metal-ligating amino acid side chains, including seven histidines arranged in motifs characteristic of metalloproteins and metallopeptides. Notably, Hist-5 displays an **A**mino **T**erminal **Cu**(II), **Ni**(II) binding motif (ATCUN; H_2N-X-X-His),[16–17] a His-Glu-X-X-His Zn(II)-binding motif, and a *bis*-His motif composed of adjacent histidines and that supports Cu(I) binding.[18–20] The characteristic structures of Cu bound to ATCUN and *bis*-His motifs is shown in Fig. 1.

Metal-binding properties of Hist-5 have been proposed for nearly two decades,[15, 21–22] and its metal-binding interactions with Cu(II), Ni(II), Zn(II) and Fe(III) have been investigated in vitro.[21–26] Metal binding has been observed to modify the conformation and biological activity of Hist-5. Whereas binding to divalent ions like Cu(II), Ni(II) and Zn(II) was not found to stabilize secondary structure of Hist-5,[27] binding to Fe(III) has been shown to induce an α-helical conformation.[22] At least one study showed that supplemental Zn(II) improved the bactericidal activity of Hist-5,[28] while other studies showed no effect of Zn on Hist-5 candidacidal activity.[22] On the other hand, Fe supplementation was observed to decrease the in vitro candidacidal activity of Hist-5, and Hist-5 itself caused a decrease in expression levels of iron uptake genes in *C. albicans*.[22]

The effects of Cu on the antifungal activity of Hist-5 have not been explicitly studied, although several reports in the literature speculate on a possible role of Cu redox chemistry on Hist-5 activity. For example, hydrogen peroxide was detected from aqueous solutions of Cu(II), Hist-5 and ascorbic acid, raising the intriguing possibility that Cu-Hist-5 complexes can catalyze ROS generation.[29–31] The fact that yeast mitochondria have been shown to have a non-proteinaceous pool of copper in the mitochondrial matrix,[32] where Hist-5 localizes, suggests ROS production as a feasible mechanism involved in killing.

To date, a lack of biological and chemical data to support or refute the hypothesis that Cu plays an important role in Hist-5 antimicrobial activity represents a significant gap in knowledge. Data on the coordination structures and binding affinities of both Cu(II) and Cu(I) interactions with Hist-5 and whether Cu sites are required for Hist-5 activity is crucial for understanding the chemical details of Hist-5's biological activity. Although Cu interactions with Hist-5 and its model peptides have been investigated previously, the published affinity constant for interaction between Cu(II) and the ATCUN site of Hist-5 is surprisingly low ($K_{Hist\text{-}5\text{-}Cu(II)} = 2.6 \times 10^7$)[15] compared to values characterized for other ATCUN peptide systems ($K_{Cu(II)P}$ values ranging from $10^{11} – 10^{15}$).[19, 33–35] To the best of our knowledge, the potential interactions between Hist-5 and Cu(I) have not been investigated. Further, it is unknown what effect, if any, Cu binding sites have on the antifungal activity of Hist-5.

Here, we reevaluate the Hist-5 Cu(II) affinity constant using methods similar to those that have recently been published for similar ATCUN-containing peptide systems.[19, 33] We also present new evidence of the affinity and coordination structures of Hist-5 Cu(I) binding. Additionally, we characterize the potential role of Cu in Hist-5 candidacidal activity and present the first evidence that Cu availability improves growth inhibition of *C. albicans* by

Hist-5 in fungal growth assays. Furthermore, we show that the first twelve amino acids of Hist-5 retain significant antifungal activity in a Cu-dependent fashion, whereas modification of key Cu-binding residues abrogates activity. Interestingly, the Cu-dependent growth inhibition correlates with the presence of a *bis*-His site and the affinity of the peptides for Cu(I). These findings reveal the importance of Cu and Cu-binding motifs for the antifungal activity of Hist-5, providing further evidence for the involvement of metals in modulating the biological activity of histatin antifungal peptides.

Results

Hist-5 and a series of truncated peptides based on its first 12 amino acids were synthesized via Fmoc solid-phase peptide synthesis. Truncated peptides with His-to-Ala substitutions were prepared in order to probe the importance of His residues on Cu(II) and Cu(I) binding affinity and antifungal activity; names and sequences are shown in Table 1.

ATCUN site confers Hist-5 with high affinity for Cu(II)

Addition of $CuSO_4$ to buffered solutions of Hist-5 resulted in an absorption band centered at 530 nm (ε = 110 $M^{-1}cm^{-1}$), indicative of a square-planar, 4N-coordination environment of Cu(II) bound in an ATCUN site, as drawn in Fig. 1.[36] Nearly identical absorption bands were observed for all the peptides except H3A, which resulted in an absorbance redshift to ~ 620 nm (Fig. 2).

Determination of the apparent affinity constants at pH 7.4 for Cu(II) binding to each peptide was facilitated by using nitrilotriacetic acid (NTA) as a competitive ligand (Fig. 3), an appropriate methodology for determining metal–protein or peptide affinities.[37] Hist-5 was determined to bind Cu(II) with an apparent log $K_{Hist\text{-}5\text{-}Cu(II)}$ of 11.1 ± 0.2 (K_d ~ 8 pM). While direct titration of Hist-5 with Cu(II) indicated that Hist-5 is capable of binding more than one equivalent of Cu(II), as reported by others,[15] the competition studies showed that none of these additional sites are strong enough to compete with NTA for Cu(II). As shown in Table 1, neither truncation to the first 12 residues nor replacement of His 7 and 8 diminished Cu(II) affinity. Peptide H3A, on the other hand, did not compete for Cu(II) with NTA, therefore its affinity is too weak to be measured by this method. Together these results confirm that Hist-5 binds Cu(II) preferentially via the ATCUN site, regardless of other potential metal-binding residues present, and altering this site drastically decreases its Cu(II) affinity.

The bis-His motif contributes to Cu(I) binding of Hist-5 peptides

Apparent binding affinities for Cu(I) were determined anaerobically by using Ferrozine (Fz) as a colorimetric competitive ligand (Fig. 4). Addition of Hist-5 caused a decrease of the characteristic $[Cu(I)(Fz)_2]^{3-}$ absorption bands at 470 and 610 nm, indicating competition between the peptide and Fz for Cu(I). A weak feature observed late in the titration at 568 nm indicates formation of $[Fe(II)(Fz)_3]^{4-}$ due to trace iron, as has been observed previously.[18] Data were corrected for this contribution. These data show that Hist-5 is the best at competing with Fz for Cu(I), with the truncated peptides retaining Cu(I) binding affinity that

varies depending on the presence and position of His residues. Titrations done in both directions (peptide to $Cu(Fz)_2$ and Fz to Cu(peptide) returned similar results (Fig. S2).

Stoichiometry of binding was assessed by fitting titration data to multiple peptide:Cu binding models, including 1:1, 1:2 and 2:1, as shown in Fig. S3, with final log K values tabulated in Table 1. Of the peptides tested, only Hist-5 displayed a 1:2 peptide:Cu(I) binding complex, likely due to the presence of two *bis*-His motifs, to give an overall log $K_{P:2Cu(I)}$ of 15.4 ± 0.2. A reverse titration of Fz into a 1:1 solution of Cu(I):Hist-5 provided log $K1_{PCu(I)}$ of 7.8 ±0.2 for the first site, allowing for calculation of the second site to be log $K2_{PCu(I)}$ of 7.6 ± 0.3. These similar values correspond to dissociation constants (K_d) for each *bis*-His Cu(I) site between 16–25 nM.

The truncated peptide Hist 1–12 was best fit by a 1:1 peptide:Cu(I) binding model with an apparent log $K_{P:Cu(I)}$ of 7.1 ± 0.3 (K_d = 79 nM), a value slightly weaker than the individual binding sites of the full-length Hist-5. If this binding site were comprised exclusively of the *bis*-His motif, H3A would be expected to return a similar value, yet the best fit 1:1 binding model yields a weaker K_d of 200 nM, suggesting that the histidine at the third position facilitates strong Cu(I) coordination at the *bis*-His site. The importance of maintaining the adjacent His residues for effective Cu(I) binding by histatin peptides is highlighted by the fact that eliminating both of them rendered peptide H7,8A incapable of competing for Cu(I) from Fz, while eliminating just one of them (H7A) gave a peptide that only weakly competes with Fz for Cu(I), and does so by forming a 2:1 peptide:Cu(I) complex.

Overall, these spectroscopic data show that the histidine-rich sequence of Hist-5 supports Cu(I) coordination via its *bis*-His motifs, with potential contribution from an additional His.

X-ray absorption spectroscopy reveals that His3 is involved in coordination of Cu(I) at the bis-His site

To confirm the presence of a Cu(I) binding site in the histatin peptides, samples of Cu(I) loaded Hist 1–12, H3A, and H7,8A were analyzed using X-ray absorption spectroscopy. Fig. 5a compares the X-ray absorption near edge spectra (XANES) for the three peptide complexes. XANES spectra of Cu are quite sensitive to coordination number and oxidation state, as described by Kau et al.[38] In particular, the presence of a prominent 1s-to-4p feature at ~8984 eV (vertical line) and the absence of a 1s-to-3d transition unambiguously indicate that the peptides are all binding Cu(I). The intensity of these features relative to the total edge height is inversely proportional to the coordination number. Two-coordinate near linear geometries typically have intensities equivalent in magnitude to the main edge.[38] The Hist 1–12 peptide samples evaluated had amplitudes between 0.6–0.8 relative to the edge that is normalized to 1. Fig. 5a shows the sample with the highest intensity we observed; it has a magnitude between the intensity values reported for pure 2 coordinate (~1.0) and pure 3 coordinate (~0.6) compounds.[38] In the compounds evaluated by Kau et al, the only three coordinate complex with a 1s-to-4p transition with this magnitude of 0.8 was a T-shaped coordinate system with short 1.87 Å Cu–N bond lengths. The H3A peptide complexes consistently had a slightly higher amplitude of the edge feature at 8984 eV than did the Hist1–12 peptide complexes. The XANES spectrum for the H7,8A peptide where the *bis*-His binding site is removed still indicates the presence of Cu(I), but there are clearly

structural changes that have occurred relative to Hist 1–12 and H3A. Addition of more equivalents of Cu(I) to any of the peptides dramatically changed the edge structure, indicating that other sites on the peptide may provide additional (possibly adventitious) binding sites for Cu(I) (data not shown). Interestingly, addition of H_2O_2 to Hist 1–12 results in the loss of the 8984 eV feature and a shift to higher edge energy, indicating that the geometry allows for redox activity (data not shown).

To validate that the Hist 1–12 peptide forms a three coordinate Cu(I) complex, we compared the x-ray absorption fine structure (EXAFS) of Hist 1–12 and H3A. The Fourier transformed (FT) data of both peptides indicate the presence of substantial histidine scatterers, as evidenced by the prominent peaks between 2–4 Å in the FT (Fig. 5b–c). Fits of the Hist 1–12 data indicate the presence of two sub-shells of nearest neighbors, 2 N/O at 1.90 Å and another low-Z ligand at 2.11 Å (Table S1). The disorder of the longer nearest-neighbor subshell is evident in the higher Debye-Waller factor, σ^2, but in most categories of fits evaluated, addition of the extra first shell ligand improved the fit and refined consistently to the same value. Addition of shells of scatterers from the carbon/nitrogen in the ordered histidine rings improves the fit (Table S1) and the best five shell fit is shown in Fig. 5b and is indicated in bold on Table S1.

In contrast to Hist 1–12, the H3A peptide can best be fit with just the single short first shell ligand set at 1.90 Å. If an additional sub-shell of nearest neighbors is added to the model, the fit refines with a longer distance (2.3 Å) and an unrealistically high value for the bond disorder. The Cu–N distance still refines to the value of 1.90 Å, indicating that a third ligand, possibly from solvent, is likely present but is not well ordered enough to be refined. The intensity of the pre-edge feature and the first shell distance again suggest that H3A may have a third disordered ligand, though one distinct from that present in Hist 1–12. Pure two coordinate *bis*-His coordination is expected to yield a slightly shorter Cu–N distance of 1.86–1.88 Å; the edge feature at 8984 eV would also be expected to be more intense.[20, 39–40] Other structural changes in the histidine scattering region are evident when comparing the FTs of Hist 1–12 and H3A, suggesting that the His3 may be involved in the binding of Cu(I) in Hist 1–12. Fig. 5c shows the best four shell fit for the H3A peptide, indicated in bold in Table S1.

Metal-binding motifs affect antifungal activity of Hist-5

Antifungal susceptibility assays were performed to evaluate the effect of supplemental Cu(II) and Fe(III) on the antifungal activity of Hist-5. The *C. albicans* yeast cells treated with Hist-5 alone exhibited an EC_{50} of 5.15 μM (Fig. 6a, **black bars**), while co-treatment with 100 μM $FeCl_3$ rendered Hist-5 ineffective at inhibiting growth (Fig. 6a, **red bars**). In fact, low μM Fe(III) was sufficient to cause a decrease in activity (Fig. 6b and S6). Contrary to Fe(III), the addition of $CuSO_4$ caused a decrease in EC_{50} of Hist-5 to 1.36 μM (Fig. 6a, **blue bars**). Low μM concentrations of added Cu(II) were sufficient to cause a decrease in EC_{50} (Fig. 6b and S5). Neither Cu(II) nor Fe(III) by themselves inhibited growth of *C. albicans* in the concentration range tested (0–100 μM; Fig. S4a–b). It is worth noting that increasing concentrations of both of these metal ions increased the lag phase of *C. albicans*, as expected for a change in growth environment that includes high metal levels.[41] Taken

together, these metal supplementation data reveal that Fe and Cu both potentiate the antifungal activity of Hist-5, but in *opposite* directions, with Fe abrogating activity and Cu facilitating activity.

To evaluate the relevance of the Cu-binding sites on antifungal activity, a series of mutant full-length Hist-5 peptides were tested (Table 2). Replacement of the ATCUN or either of the two *bis*-His motifs caused an increase in the EC_{50} to 15.8, 13.0 and >100 μM (Hist-5(H3A), Hist-5(H7,8A), and Hist-5(H18,19A), respectively). Co-treatment with Fe(III) inhibited the antifungal activity of all the full-length mutants, as observed with Hist-5. Contrary to Fe(III), supplementing with Cu(II) caused a decrease in EC_{50} values for Hist-5(H3A) and Hist-5(H18,19A) to be ~5.00 and 1.35 μM, respectively. Strikingly, Hist-5(H7,8A) remained ineffective at all concentrations tested, even with Cu treatment. Whereas loss of the H^{18},H^{19} *bis*-His site only mildly modulates antifungal activity compared to Hist-5, the complete loss of activity for the mutant lacking H^{7},H^{8} emphasizes the importance of the *bis*-His motif most proximal to the ATCUN motif. Furthermore, Hist-5(H18,19A) exhibits a similar EC_{50} upon Cu treatment to that of Hist-5, therefore suggesting the importance of the most proximal *bis*-His site in Cu-potentiated activity.

Unlike the full-length peptides, none of the truncated peptides alone exhibited an EC_{50} below 25 μM (Table 2). Co-treatment with Fe(III) did not have any observable effect on growth, which is not surprising given that they were not active on their own at the concentrations tested. Interestingly, however, co-treatment of peptides with Cu(II) revealed EC_{50} values for Hist 1–12, H3A and H7A to be ~5, 6, and 14 μM, respectively. Peptide H7,8A, on the other hand, remained ineffective at all concentrations tested, regardless of Cu treatment. The minimal difference in EC_{50} for Hist 1–12 compared to H3A suggests that His3 is not critical for antifungal activity. The finding that H7A is less effective and H7,8A is completely ineffective suggests the importance of an intact *bis*-His motif for the Cu-dependent antifungal activity of the truncated Hist-5 peptides. The results obtained with the truncated peptides uphold the results obtained with the full-length mutant peptides, further suggesting the importance of the *bis*-His motif for the Cu-dependent antifungal activity of Hist-5.

The metal dependence of Hist-5 antifungal activity was further tested by co-treating cells with peptides and either bathocuproine disulphonate (BCS), a cell impermeable chelator frequently used to limit Cu availability in cell culture, or ethylenediaminetetraacetic acid (EDTA), a general metal ion chelator. Initial susceptibility testing of the ligands alone showed that concentrations at or below 2 mM BCS and 0.25 mM EDTA were well tolerated by *C. albicans* (Figs. S4). Co-treatment with peptides and 2 mM BCS completely abrogated the growth inhibitory activity of Hist-5 (Fig. 6a, **purple bars**), whereas 0.25 mM EDTA caused an increase in EC_{50} to 22.5 μM (Fig. 6a, **green bars**). These results bolster the Cu-supplementation results and further support the concept that Cu availability influences the antifungal activity of Hist-5.

To buttress the assumption that the effect of BCS on the antifungal activity of Hist-5 is due to BCS competing with Hist-5 for binding Cu, a solution of 7 μM Hist-5 and 7 μM $CuSO_4$ was prepared in YPD medium and incubated with varying concentrations of BCS for 1 h. As

observed in Fig. 7, the characteristic Cu(II)-ATCUN absorption feature (~ 530 nm) was not detected at the concentration analyzed of the Cu-bound Hist-5 complex. Addition of BCS resulted in the dose-dependent formation of an absorption band ~ 483 nm (ε = 13,300 $M^{-1}cm^{-1}$),[42] indicative of the $[Cu(BCS)_2]^{3-}$ complex. At 2 mM BCS, the calculated concentration of $[Cu(BCS)_2]^{3-}$ complex based on its absorbance at 483 nm was 7.3 μM. This concentration matches the 7.0 μM Cu added in solution together with basal Cu concentration of the YPD media (0.27 ± 0.04 μM, as determined by ICP-MS) indicating that all Cu has been reduced and sequestered as the Cu(I)-BCS complex. These results corroborate that under the 2 mM BCS conditions used in the antifungal assays, Cu is not available to Hist-5.

In order to test the fungicidal activity of Hist-5, *C. albicans* were incubated overnight in YPD (normal protocol) or in YPD supplemented with 100 μM $CuSO_4$ or 2 mM BCS. ICP-MS was used to verify the cell-associated Cu content for each of the conditions. Cells grown under these basal, Cu-replete or Cu-depleted conditions (1, 126 and 0.3 Cu/mg P, respectively) were then washed to remove the treatments before exposure to Hist-5 alone or with 2 mM BCS for 1.5 h in buffer before plating on fresh agar and grown overnight. As shown in Fig. 8b, this killing assay (spot test) confirmed that Hist-5 is fungicidal above 6 μM, whereas co-treatment with BCS prevented the fungicidal activity (Fig. 8b, II vs. I). Notably, the Cu content for cells grown under these conditions were the same, within error (Fig. 8a, II vs. I). Cells grown overnight with BCS, however, showed a 70% decrease in cell-associated Cu compared to the basal level (0.308 vs 1.0 nmol Cu/mg P, respectively). Under these conditions, Hist-5 was not fungicidal at the concentrations tested, although growth was lower compared to BCS co-treatment condition (Fig. 8b III vs. II). In contrast, cells grown under Cu-replete conditions were sensitized to Hist-5 toxicity (Fig. 8b, IV). Taken together, these data support a model in which Hist-5 uses available Cu to enhance its fungicidal activity. Hist-5 may acquire its Cu cofactor from trace Cu in surrounding medium, supplemental Cu intentionally added, or cell-associated Cu.

Discussion

Hist-5 has been previously shown to have metal binding capabilities, including for Cu(II). Yet the relevance of Cu binding to Hist-5 antifungal activity has not previously been established and biological and spectroscopic evidence to support claims of metal-associated activity are lacking. The work presented here provides evidence that the histidine-rich sequence of Hist-5 confers the salivary peptide with high affinity for Cu in both Cu(I) and Cu(II) oxidation states. X-ray absorption spectra indicate that both Hist 1–12 and H3A bind Cu(I) using the *bis*-His binding site, as evidenced by substantial histidine scattering in the EXAFS and by the prominent pre-edge feature that results from a 1s-4p transition in Cu(I). Most importantly, the antifungal data collected on full-length Hist-5 and several His-to-Ala mutant and truncated peptides provides the first evidence that links the Cu binding capability of histatin peptides with their antifungal activity against *C. albicans*.

Competition titration data indicated that Hist-5 binds Cu(II) in an ATCUN site with apparent $K_{Hist\text{-}5\text{-}Cu(II)}$ of approximately 10^{11} (K_d ~ 8 pM). This affinity for Cu(II) is significantly higher than the value previously reported for Cu(II) binding to Hist-5 ($K_{Hist\text{-}5\text{-}Cu(II)}$ = 2.6 ×

10^7),[15] however it is more in line with the value that would be expected based on similar analysis of ATCUN sites in human albumin ($K_{albumin\text{-}Cu(II)} = 10^{12}$)[33] and models of the human copper transporter (Ctr1, $K_{Ctr1\text{-}Cu(II)} = 10^{11}$).[19] Our results are in significant disagreement with Gusman et al, and we suggest that the conditional nature of the reported values and the difference in methodology can explain why these values differ by approximately four orders of magnitude. The competition equilibrium methodology used here minimizes many of the problems that can plague the determination of metal-protein affinities, including metal hydrolysis and binding to adventitious sites and buffer components.[37] Gusman et al employed isothermal titration calorimetry in cholamine chloride buffer in determining $K_{Hist\text{-}5\text{-}Cu(II)}$. Cholamine chloride is a Good's buffer, however Good's buffers are not completely innocent in interactions with all metal ions.[43] Cholamine chloride has a primary amine functional group capable of significant interaction with Cu(II), and to our best knowledge, the interactions of this buffer with Cu(II) have not been characterized. HEPES buffer is also a Good's buffer that is non-innocent in its interactions with Cu(II), but it is recommended[43] for study of Cu(II) interactions with biological ligands because interactions between Cu(II) and HEPES are fully characterized.[44] HEPES is the buffer that was used here, and in the determination of Cu(II) affinity with albumin and Ctr1 referenced above.[19, 33] We note that the reported value for albumin is a conditional constant in which contributions of HEPES buffer interactions with Cu have been accounted for. However, in the case of the reported values for Cu(II) binding to Ctr1 model peptide, and here for Hist-5, HEPES buffer contributions are ignored. Thus, although these three ATCUN-containing polypeptides were examined under similar conditions, the values for Hist-5 and Ctr1 model peptides can be directly compared, but should not be directly compared to that of albumin. If buffer contributions are accounted for in the latter two cases, all three systems retain nearly identical affinities.[44] The comparable affinities of Hist-5 and other ATCUN-Cu(II) peptides and proteins suggests that Hist-5 would be capable of competing with Cu(II) binding proteins in saliva, which include albumin.

While Cu would not be expected to exist extracellularly as Cu(I), the presence of reductants or any redox cycling of Cu-bound histatin would provide sources of Cu(I). Our results indicate that the *bis*-His motifs contribute to moderate, nanomolar affinity of histatin peptides for Cu(I). *Bis*-His sites have been shown to bind Cu(I) in other systems, including amyloid-β, with ~130 nM affinity,[18] and model peptides of the copper transport protein, human Ctr1, with sub-nanomolar affinity.[39, 45] Additional Met or His ligating residues were postulated to complement the *bis*-His Cu(I) binding site in the human Ctr1 peptides and the data here also suggest that additional ligating residues may complement the *bis*-His site in histatins.

Indeed, fits to Hist 1–12 indicate that a third ligand is present as a nearest neighbor. The 1.90 Å distance refined for the *bis*-His Cu–N distances is slightly outside the normal window for pure two coordinate *bis*-His binding.[20] EXAFS distances do have an uncertainty of ± 0.02 Å due in part to the strong correlation of distance with the chosen value of E_0, the threshold energy; this leaves open the possibility that our longer distance is, within the error of the measurement, indicative of a two-coordinate complex. However, we note that ΔE_0 must be forced to an unusually high value in order to tweak the distance down to 1.88 Å in a fit; these high ΔE_0 values are inconsistent with both our own calibration of ΔE_0 values and those

reported by others using the same modeling programs.[39] In addition, the magnitude of the 1s-to-4p transition at ~8984 eV ranges from 0.6 to 0.8 in the samples we evaluated and these magnitudes are more indicative of a three coordinate Cu(I) complex.[38] Two coordinate Cu(I) *bis*-His ligation in Amyloid-β peptide fragments and human prion protein fragments both refined to shorter Cu–N distances (1.88 Å) and typically have higher pre-edge intensities.[20, 39–40] Finally, if the coordination of Cu(I) in Hist 1–12 and H3A were only reliant on the two adjacent His residues as ligands, then we would expect the EXAFS spectra of these peptides to be identical, and they are not. There are in fact subtle changes in the EXAFS both in the first shell and in the outer shells where histidine backscattering predominates. For H3A, the third ligand is very disordered and a clean minimum cannot be found for this subshell with the fits. In addition, there are visible changes associated with the histidine peaks in the FT when His3 is absent. The structural differences apparent in the EXAFS for Hist 1–12 and H3A and the binding differences evident in the K_d values suggest that the third ligand for Hist 1–12 may be provided by His3.

The spectroscopic results illustrating the strong binding affinity of Hist-5 for Cu(I) and Cu(II) raise the question of whether Cu plays a role in its activity. We therefore speculated that the antifungal activity of Hist-5 may be modulated by the availability of metals in general, and copper specifically.[46–48] Indeed, the presence or absence of Cu(II) and Fe(III) dramatically affected the activity of Hist-5 and its derivatives against *C. albicans*. The loss of Hist-5 antifungal activity in the presence of Fe(III) confirmed prior reports.[22] Interesting to us, however, was the improvement in candidacidal activity of Hist-5 supplemented with Cu, shifting the EC_{50} from 5.15 μM to 1.36 μM. Conversely, inclusion of the extracellular copper chelator BCS completely rescued *Candida* growth at otherwise inhibitory concentrations of Hist-5.

The Cu-modulated activity of Hist-5 has several possible explanations. The apparent Cu-facilitating activity could be a coincidental result of Hist-5 and Cu levels affecting different but interconnected cellular processes. Alternatively, Hist-5 and Cu could directly interact to create a toxicity-inducing complex. The observation that antifungal activity of the “mutant” peptides correlated with their physical ability to bind Cu(I) provides some evidence favoring a direct interaction. Basal levels of Cu in the growth medium or *in situ* may supply Hist-5 with sufficient Cu cofactor for activity. The observation that cells cultured in Cu-replete medium were sensitized to Hist-5 activity supports this idea (Fig. 8b). Alternatively, Hist-5 may have both Cu-dependent and independent mechanisms of action. Cu supplementation may boost a Cu-dependent mechanism, thus a decrease in EC_{50}.

The lack of Hist-5 candidacidal activity observed when co-treated with BCS would seem to favor a Cu-dependent mechanism. However, an alternative explanation could be that *C. albicans* undergoes metabolic adaptations to a Cu deprived environment created by BCS that reduces its susceptibility to Hist-5. Cu deficiency is known to limit fungal cell growth and leads to down-regulation of respiratory function, presumably to preserve Fe and Cu for the most critical cellular processes.[49] In addition, Cu limitation inhibits cytochrome oxidase expression, thereby limiting mitochondrial respiration.[50–51] It has been shown that anaerobic conditions and metabolic inhibitors protect *C. albicans* against Hist-5.[13] Therefore, BCS may be reducing or inhibiting respiratory function by depleting Cu, thereby rendering Hist-5

ineffective.[52] The results of the ICP-MS and spot assay in Fig. 8a,b, however, showed that exposure to 2 mM BCS for 1.5 h does not deplete cellular Cu levels, but does abrogate activity of Hist-5, suggesting that cellular Cu-deficiency itself is not the primary driver behind the effect of BCS on Hist-5 activity. Consistent with the results from Fig. 6, the effect of BCS was most pronounced when cells were exposed to Hist-5 and BCS *at the same time*, suggesting that BCS diminishes Hist-5 activity by withholding or competing Cu away from a direct interaction with Hist-5, as observed in Fig. 7. Combined, these results support a model that invokes Cu as a cofactor necessary for optimal antifungal activity of Hist-5.

Several studies have explored amino acid sequence requirements for the antifungal activity of Hist-5.[8, 25, 53–59] Among a series of histatin fragments, C-terminal peptides with chain lengths greater than 14 residues were found to retain activity similar to full length Hist-5, while N-terminal fragments were less active.[8] Among other variations in experimental design, that study did not test the effect of Cu or other metals on activity, although all of the active fragments did contain at least one *bis*-His motif. In the current study, we also found that N-terminal fragments showed diminished activity, in fact, a maximum concentration of 100 μM Hist 1–12 failed to inhibit the growth of *C. albicans*. However, addition of Cu restored activity of Hist 1–12 to levels approaching full-length Hist-5. Furthermore, we found that mutating the H^7,H^8 *bis*-His site of the full-length Hist-5 mutant rendered the peptide ineffective, whereas eliminating $H^{18}H^{19}$ *bis*-His site retained activity. Based on our series of N-terminal truncated and full-length mutant peptides, Cu-dependent activity depends on a *bis*-His motif, particularly the H^7H^8 site, but not an ATCUN site.

Bis-His motifs are commonly found in biological systems, and have been observed to bind Cu(I) in a linear fashion, while also accommodating an additional ligand. The coordination motif has been shown to grant Cu(I)-*bis*-His complexes with O_2 reactivity, leading to the generation of ROS.[20, 39–40, 60] Our XAS results corroborate a similar Cu(I)-coordination mode by the histatin-derived peptides, suggesting that the Cu(I)-histatin complex could potentially mediate Cu-induced ROS, which in turn could elicit fungal killing. Altogether, the XAS and antifungal assay results suggest that the *bis*-His site may not only serve as a primary anchor for Cu(I) binding, but, once bound to Cu(I), may also be directly responsible for the antifungal activity of Histatin-5. This speculation will require further experimental testing.

The results here provide evidence that Cu contributes to the antifungal activity of histatin peptides, but *how* Cu contributes to its mechanism of action remains an open question. Perhaps its ability to stabilize both Cu(I) and Cu(II) endows it with unique redox properties,[45] a hypothesis we are currently exploring.

Experimental Section

Peptide synthesis and purification

All peptides were synthesized on a Protein Technologies PS3 automated peptide synthesizer using Fmoc-L-Tyr(tBu)-Wang or rink amide MBHA resins (Chem-Impex Int'l Inc.) in 0.1 mmol scale. Amino acid coupling was achieved using HBTU (O-benzotriazole-N,N,N',N'-tetramethyluronium hexafluorophosphate; Chem-Impex Int'l Inc.) in the presence of N-

methylmorpholine in N,N'-dimethylformamide (DMF) for 30 min cycles. Fmoc deprotection was accomplished with the use of 20% piperidine in DMF. Side chain deprotection and peptide cleavage from the resin were achieved by treating with 5 mL of a solution of 95% trifluoroacetic acid (TFA), 2.5% ethane dithiol, and 2.5% triisopropylsilane (TIS, Sigma-Aldrich) for 4 h under N_2 gas to yield peptides with N-terminal free amines and C-terminal carboxylic acids for Hist-5 and C-terminal amide for model peptides. A continuous flow of N_2 gas was used to evaporate TFA to a volume of 2 mL. Afterwards, peptide was precipitated and washed three times with diethyl ether (Sigma-Aldrich), and left to air-dry. Peptides were purified using semi-prep reverse-phase HPLC on a C-8 column with a 40 min linear gradient from 3–97% acetonitrile in water, with 0.1% TFA. Purity was validated to >95% by analytical HPLC, and the masses of the peptides were confirmed by ESI-MS. Hist-5 calculated for 3036.3: Found ($M+2H^+$) 1518.2. Hist-5(H3A) calculated for 2970.2: Found (M+2H) 1483.1. Hist-5(H7,8A) calculated for 2904.1: Found (M+2H) 1452.3. Hist-5(H18,19A) calculated for 2904.1: Found (M+2H) 1452.1. Hist 1–12 calculated for 1490.6: Found ($M+H^+$) 1490.7. H3A calculated 1424.6: Found ($M+H^+$) 1424.6. H7A calculated 1424.6: Found ($M+H^+$) 1424.9. H7,8A calculated 1358.5: Found ($M+H^+$) 1359.1.

Preparation of stock solutions

Peptide stock solutions were prepared by dissolving lyophilized peptide in 1 mL of nanopure water. Concentration of stock solutions was determined using the Edelhoch method.[61] In short, 4–6 μL of peptide stock were diluted into 400 μL of 8 mM urea to obtain an absorbance at 280 nm between 0.1 and 1 absorbance unit. The concentration of the peptide solution was determined from the A_{278nm} readings using an extinction coefficient of 1450 $M^{-1}cm^{-1}$ for each tyrosine.[62] Peptide stock solutions were stored in sealed cryogenic storage vials. Copper(II) stock solutions were prepared by dissolving copper sulfate ($CuSO_4$, Sigma) in nanopure water and standardized by EDTA titration in an ammonium buffer to a murexide endpoint. Copper(I) solutions were prepared by dissolving $[Cu(CH_3CN)_4]PF_6$ (Aldrich) in anhydrous acetonitrile (Fisher) and subsequently standardized with the use of the chromophoric ligand bicinchoninate (BCA). The concentration of Cu(I) solutions was determined from the absorption at 563 nm due to the $Cu(I)(BCA)_2$ complex (ε = 7900 $M^{-1}cm^{-1}$).[63]

UV-Vis spectroscopy

Absorption spectra were recorded in 1-cm quartz cuvettes on a Varian Cary 50 UV-Visible spectrophotometer for studies with Cu(II). All spectrophotometric experiments using Cu(I) were conducted on an SI Photonics model 420 fiber optic CCD array spectrophotometer located inside a Siemens MBraun glove box under inert N_2 atmosphere.

Determination of peptide-copper binding constants

Apparent association constants for Cu(I/II) binding were determined in 50 mM HEPES buffer at a pH of 7.4, as described in the Supp. Info. The association constants were determined by fitting the adequate binding equilibrium models using GraphPad Prism software.[64]

Cu(II) apparent binding constants

Nitrilotriacetic acid (NTA) was used as a competitive ligand to obtain apparent binding constants for peptide–Cu(II) complexes in 50 mM HEPES buffer, pH 7.4 from spectrophotometric titration data. Aliquots (0.75 μL) of peptide stock solution were titrated into solutions containing 1 mM NTA and 0.8 mM $CuSO_4$ to establish the exchange equilibrium expressed by Eq. 1 below (derived from the competing equilibria expressed in Eqs 3–6. The concentration of NTA(Cu(II)) at each point in the titration was calculated from the characteristic visible absorbance of NTA(Cu(II)) at 800 nm (ε = 64 M^{-1} cm^{-1}). Reverse titrations were also carried out by titrating NTA into solutions containing peptide and $CuSO_4$. Calculations of the other species present in solution were calculated from mass-balance equations. Data plotted as [NTA(Cu(II))] vs. $[peptide]_{total}$ were fit to the equilibrium model shown in Eq. 2 using GraphPad Prism software[64] to obtain K_{ex}. The desired $K_{P(Cu(II))}$ was then calculated from Eq. 2 using the known value for NTA (log $K_{NTA(Cu(II))}$ = 10.68, pH 7.4).[65] Log K values shown in Table 1 represent the average and standard deviation obtained from triplicate titration experiments.

$$NTA + P(Cu(II)) \leftrightarrow NTA(Cu(II)) + P \quad (1)$$

$$K_{ex} = \frac{K_{NTA(Cu(II))}}{K_{P(Cu(II))}} = \frac{[NTA(Cu(II))[P]}{[NTA][P(Cu(II))]} \quad (2)$$

$$P + Cu(II) \leftrightarrow P(Cu(II)) \quad (3)$$

$$K_{P(Cu(II))} = \frac{[P(Cu(II))]}{[Cu(II)][P]} \quad (4)$$

$$Cu(II) + NTA \leftrightarrow NTA(Cu(II)) \quad (5)$$

$$K_{NTA(Cu(II))} = \frac{[NTA(Cu(II))]}{[Cu(II)][NTA]} \quad (6)$$

Cu(I) apparent binding constants

All experiments with Cu(I) were performed in a N_2-filled anaerobic glove box. All buffers and reagents were degassed under N_2, sealed and transferred to the glove box. Ferrozine (Fz) was used as a competitive ligand to calculate apparent binding constants for peptide–Cu(I) complexes in 50 mM HEPES buffer, pH 7.4 from spectrophotometric titration data. Aliquots

(2.75 μL) of peptide stock solution were titrated into solutions containing 132 μM Fz and 55 μM $Cu(CH_3CN)_4PF_6$ to establish the exchange equilibrium expressed by Eq. 7 below (derived from the competing equilibria expressed in Eqs 8–12. The concentration of $Cu(Fz)_2$ complex at each point in the titration was calculated from its characteristic visible absorbance at 470 nm (ε = 4,320 M^{-1} cm^{-1}).[18, 66] Calculations of the other species present in solution were calculated from mass-balance equations. Data plotted as $[Cu(Fz)_2]$ vs. $[peptide]_{total}$ were fit to equilibrium models shown in Eq. 2 using GraphPad Prism software[64] to obtain K_{ex}. In Eqs. 7–14, *m* and *n* stand for the stoichiometric values for the component, which varies depending on the binding model. The desired $K_{P(Cu(II))}$ was then calculated from Eq. 2 using the known value for Fz ($\log K_{Fz2Cu(I))} = 11.56$, pH 7.4).[18]

$$mP + nCu(I)(Fz)_2 \leftrightarrow P_m(Cu(I))_n + 2nFz \quad (7)$$

$$K_{ex}^{mP:nCu(I)} = \frac{\left(\beta_{Cu(I)(Fz)_2}\right)^n}{K_{P_m(Cu(I))_n}^{app}} = \frac{[Cu(I)(Fz)_2]^n[P]^m}{[Fz]^{2n}[P_m(Cu(I))_n]} \quad (8)$$

$$mP + nCu(I) \leftrightarrow P_m(Cu(I))_n \quad (9)$$

$$K_{mP:nCu(I)} = \frac{[P_m(Cu(I))_n]}{[Cu(I)]^n[P]^m} \quad (10)$$

$$Cu(I) + 2Fz \leftrightarrow Cu(I)(Fz)_2 \quad (11)$$

$$\beta_{Cu(I)(Fz)_2} = \frac{[Cu(I)(Fz)_2]}{[Cu(I)][Fz]^2} \quad (12)$$

Correction for $[Fe(II)(Fz)_3]^{4-}$ formation

Contributions to the absorbance at 470 nm due to the formation of $[Fe(II)(Fz)_3]^{4-}$ were determined and corrected by using Eqs. 13 and 14, as previously described.[18] $[Fe(II)(Fz)_3]^{4-}$ exhibits an absorption maxima at 568 nm (ε = 25,000 M^{-1} cm^{-1}), and around 470 nm (ε = 8,600 M^{-1} cm^{-1}; absorption maxima of $[Cu(I)(Fz)_2]^{3-}$). The ε values for $[Cu(I)(Fz)_2]^{3-}$ at 470 nm and 568 nm are 4,320 M^{-1} cm^{-1} and 2,600 M^{-1} cm^{-1}, respectively.[18]

$$Abs(470\,nm) = \varepsilon_{Fe}^{470\,nm}[Fe(II)(Fz)_3] + \varepsilon_{Cu}^{470\,nm}[Cu(I)(Fz)_2] \quad (13)$$

$$Abs(568\,nm) = \varepsilon_{Fe}^{568\,nm}[Fe(II)(Fz)_3] + \varepsilon_{Cu}^{568\,nm}[Cu(I)(Fz)_2] \quad (13)$$

EXAFS data collection and analysis

All EXAFS samples were prepared in a nitrogen-filled anaerobic glovebox, and with degassed buffers and reagents. Solutions of Cu(I) with Hist 1–12, H3A, or H7,8A peptides (1 mM peptide, 0.9 mM $Cu(CH_3CN)_4PF_6$; 50 mM HEPES, pH 7.4, 30% v/v glycerol) were loaded into a lucite EXAFS sample cell wrapped in Kapton tape and flash frozen in liquid nitrogen. Spectra were collected at the Stanford Synchrotron Radiation Laboratory, beamline 9-3. The SSRL storage ring was operating at 3 GeV in top off mode with a ring current of 500 mA. Beamline 9-3 uses a focusing mirror, has Si(220) monochromator crystals, and a 13 keV energy-cutoff mirror was used to reject harmonics. Copper fluorescence was detected with a Canberra 100 element germanium detector. Samples were maintained at 10 K in an Oxford liquid helium continuous flow cryostat. A 6 micron nickel filter with a Soller-slit assembly was placed between the cryostat window and the detector to reduce scatter. The energy was calibrated by simultaneously measuring the edge spectrum of a copper foil, with the energy of the rising inflection point being assigned as 8980.3 eV. Data were analyzed using EXAFSPAK[67] interfaced with FEFF 7.0[68] for theoretical phase and amplitude functions. Single scattering models were used. ΔE0 and scale factor were set at −14 eV and 1.0 respectively, based on previous calibration to fits on model complexes.[69] The data were fit over a k range of 1–13 $Å^{-1}$ without the use of any Fourier filtering or smoothing. Spectra represent the average of 5–6 scans. The beam position was moved every 1–2 scans to a fresh unexposed area on the sample face to mitigate x-ray damage to the sample. The goodness of fit was evaluated using the F factor (a least-square deviation between data and fit) scaled for the number of variable parameters used in the fit (F' in Table S1). [A] the Cu-ligand distance, R, and the Debye-Waller factor, σ^2, were varied unconstrained for each shell in the fits. Coordination number was varied incrementally but was not freely varied in the fits.

Antifungal assays

A previously published method[3] was modified to accommodate a 96-well plate format. In short, *C. albicans* (ATCC, SC5314) cells were streaked on YPD agar plates and incubated at 30 °C for 24 h. Individual yeast colonies were subsequently picked from the plate, suspended in YPD medium and incubated for 16 h (logarithmic growth phase) at 30 °C. These yeast cell cultures were then diluted into 1 mM potassium phosphate buffer (PPB), pH 7.0, to an optical density at 600 nm (OD_{600}) of 0.07 and dispensed into wells of a 96-well plate that contained test peptides dissolved in 1 mM PPB at desired concentration ranges, with or without added metal salts or chelating agents. After incubating for 1.5 h at 37 °C with shaking (200 rpm), 10-μL aliquots of each well were added to a new 96-well plate

containing 190 μL fresh YPD medium in each well. Finally, the latter plate was incubated for 48 h at 30 °C with shaking (200 rpm) prior to reading final OD_{600}.

Spot Assay—Individual yeast colonies were picked from a YPD agar plate, suspended in YPD medium supplemented with 100 μM $CuSO_4$, 2 mM BCS, or no treatment, and incubated to logarithmic growth phase at 30 °C. These yeast cultures were then washed, resuspended and diluted to an OD_{600} of 0.07 with 1 mM PPB (pH 7.0), and dispensed into wells of a 96-well plate that contained test peptides dissolved in 1 mM PPB at desired concentration ranges. After incubating for 1.5 h at 37 °C with shaking (200 rpm), 4 μL aliquots of each well were spotted onto a YPD agar plate and incubated for 48 h at 30 °C.

ICP-MS Analysis—Overnight cultures were prepared as described above for each testing condition and grown for 16 h. 1 mL of the overnight culture was collected and transferred to an acid washed container. Cells were then washed once in PBS buffer and twice in 1 mM EDTA to remove cell surface-associated metals by centrifugation at 3000 rpm for 5 min. After washing, the cell pellets were dried at 75 °C overnight, digested in 200 μL of TraceMetal grade nitric acid (Fisher) for 30 min at 85 °C, and diluted with 200 μL of nanopure water that had been treated with Chelex resin to minimize metal contamination. Samples were analyzed using a Perkin Elmer Elan DRCII spectrometer by Mrs. Kim Hutchison at the Department of Soil Science of North Carolina State University. The data was normalized to the phosphorous content of each sample. Samples were done in triplicates.

Supplementary Material

Refer to Web version on PubMed Central for supplementary material.

Acknowledgments

S.E.C. and K.J.F. thank the NIH for supporting this work (GM084176 and GM084146-S1). S.E.C. would like to thank Duke University BioCoRE (R25-GM103765) for funding. E.B. acknowledges support from Helen Kuhn Carey and the Department of Chemistry and Physics Saint Mary's College, Notre Dame, IN. K.L.H. acknowledges support from a 2016 Cottrell Scholar Award from RCSA, a New Faculty Grant from Lilly Inc, and a CFAI Faculty Research Award from Saint Mary's College. P.R.G. acknowledges the U.S. Department of Energy, Office of Science, Office of Basic Energy Sciences (under Contract No. DE-AC02-76SF00515) for the use of the Stanford Synchrotron Radiation Lightsource, SLAC National Accelerator Laboratory. P.R.G. also acknowledges the DOE Office of Biological and Environmental Research and the National Institutes of Health, National Institute of General Medical Sciences (including P41GM103393) for supporting the SSRL Structural Molecular Biology Program. The contents of this publication are solely the responsibility of the authors and do not necessarily represent the official views of NIGMS or NIH.

ABBREVIATIONS

Hist-5	Histatin-5
ATCUN	amino terminal Cu(II) Ni(II) binding motif
ROS	reactive oxygen specie
NTA	nitrilotriacetic acid
Fz	ferrozine

XAS	x-ray absorption spectroscopy
BCS	bathocuproine disulphonate
EDTA	ethylenediaminetetraacetic acid
PPB	potassium phosphate buffer
ICP-MS	inductively coupled plasma mass spectrometry

References

1. Dale BA, Fredericks LP. Antimicrobial Peptides in the Oral Environment- Expression and Function in Health and Disease. Curr. Issues Mol. Biol. 2005; 7(2):119–133. [PubMed: 16053246]
2. Xu T, Levitz SM, Diamond RD, Oppenheim FG. Anticandidal activity of major human salivary histatins. Infection and Immunity. 1991; 59(8):2549–2554. [PubMed: 1855975]
3. Oppenheim FG, Xu T, McMillian FM, Levitz SM, Diamond RD, Offner GD, Troxler RF. Histatins, a novel family of histidine-rich proteins in human parotid secretion. Isolation, characterization, primary structure, and fungistatic effects on Candida albicans. J. Biol. Chem. 1988; 263(16):7472–7477. [PubMed: 3286634]
4. Martchenko M, Alarco A-M, Harcus D, Whiteway M. Superoxide Dismutases in Candida albicans: Transcriptional Regulation and Functional Characterization of the Hyphal-induced SOD5 Gene. Molecular Biology of the Cell. 2004; 15(2):456–467. [PubMed: 14617819]
5. Berman J, Sudbery PE. Candida Albicans: a molecular revolution built on lessons from budding yeast. Nat Rev Genet. 2002; 3(12):918–30. [PubMed: 12459722]
6. Brewer D, Hunter H, Lajoie G. NMR studies of the antimicrobial salivary peptides histatin 3 and histatin 5 in aqueous and nonaqueous solutions. Biochem Cell Biol. 1998; 76(2–3):247–56. [PubMed: 9923693]
7. Raj PA, Marcus E, Sukumaran DK. Structure of human salivary histatin 5 in aqueous and nonaqueous solutions. Biopolymers. 1998; 45(1):51–67. [PubMed: 9433185]
8. Raj PA, Edgerton M, Levine MJ. Salivary histatin 5: dependence of sequence, chain length, and helical conformation for candidacidal activity. J. Biol. Chem. 1990; 265(7):3898–905. [PubMed: 2406266]
9. Wiesner J, Vilcinskas A. Antimicrobial peptides The ancient arm of the human immune system. Virulence. 2010; 1(5):440–464. [PubMed: 21178486]
10. Helmerhorst EJ, van't Hof W, Breeuwer P, Veerman EC, Abee T, Troxler RF, Amerongen AV, Oppenheim FG. Characterization of histatin 5 with respect to amphipathicity, hydrophobicity, and effects on cell and mitochondrial membrane integrity excludes a candidacidal mechanism of pore formation. J Biol Chem. 2001; 276(8):5643–9. [PubMed: 11099499]
11. Puri S, Edgerton M. How does it kill?: understanding the candidacidal mechanism of salivary histatin 5. Eukaryot Cell. 2014; 13(8):958–64. [PubMed: 24951439]
12. Li XS, Reddy MS, Baev D, Edgerton M. Candida albicans Ssa1/2p is the cell envelope binding protein for human salivary histatin 5. J Biol Chem. 2003; 278(31):28553–61. [PubMed: 12761219]
13. Helmerhorst EJ, Breeuwer P, van ‘t Hof W, Walgreen-Weterings E, Oomen LCJM, Veerman ECI, Amerongen AVN, Abee T. The Cellular Target of Histatin 5 on Candida albicans Is the Energized Mitochondrion. J. Biol. Chem. 1999; 274(11):7286–7291. [PubMed: 10066791]
14. Helmerhorst EJ, Troxler RF, Oppenheim FG. The human salivary peptide histatin 5 exerts its antifungal activity through the formation of reactive oxygen species. Proceedings of the National Academy of Sciences of the United States of America. 2001; 98(25):14637–14642. [PubMed: 11717389]
15. Gusman H, Lendenmann U, Grogan J, Troxler RF, Oppenheim FG. Is salivary histatin 5 a metallopeptide? Biochimica Et Biophysica Acta-Protein Structure and Molecular Enzymology. 2001; 1545(1–2):86–95.

16. Sankararamakrishnan R, Verma S, Kumar S. ATCUN-like metal-binding motifs in proteins: identification and characterization by crystal structure and sequence analysis. Proteins. 2005; 58(1):211–21. [PubMed: 15508143]

17. Laussac JP, Sarker B. Characterization of the copper(II) and nickel(II) transport site of human serum albumin. Studies of copper(II) and nickel(II) binding to peptide 1–24 of human serum albumin by carbon-13 and proton NMR spectroscopy. Biochemistry. 1984; 23(12):2832–2838. [PubMed: 6547847]

18. Alies B, Badei B, Faller P, Hureau C. Reevaluation of copper(I) affinity for amyloid-beta peptides by competition with ferrozine--an unusual copper(I) indicator. Chemistry. 2012; 18(4):1161–7. [PubMed: 22189983]

19. Haas KL, Putterman AB, White DR, Thiele DJ, Franz KJ. Model peptides provide new insights into the role of histidine residues as potential ligands in human cellular copper acquisition via Ctr1. J Am Chem Soc. 2011; 133(12):4427–37. [PubMed: 21375246]

20. Himes RA, Park GY, Siluvai GS, Blackburn NJ, Karlin KD. Structural Studies of Copper(I) Complexes of Amyloid-β Peptide Fragments: Formation of Two-Coordinate Bis(histidine) Complexes. Angewandte Chemie (International ed. in English). 2008; 47(47):9084–9087. [PubMed: 18932185]

21. Grogan J, McKnight CJ, Troxler RF, Oppenheim FG. Zinc and copper bind to unique sites of histatin 5. FEBS Lett. 2001; 491(1–2):76–80. [PubMed: 11226423]

22. Puri S, Li R, Ruszaj D, Tati S, Edgerton M. Iron binding modulates candidacidal properties of salivary histatin 5. J Dent Res. 2015; 94(1):201–8. [PubMed: 25365968]

23. Kurowska E, Bonna A, Goch G, Bal W. Salivary histatin-5, a physiologically relevant ligand for Ni(II) ions. J Inorg Biochem. 2011; 105(9):1220–5. [PubMed: 21741339]

24. Kurowska E, Bonna A, Jaremko Ł, Jaremko M, Nowakowski M, Ejchart A, Bal W. Histatin-5 a salivary target for allergenic nickel(II). Toxicol. Lett. 2010; 196:S309.

25. Porciatti E, Milenkovic M, Gaggelli E, Valensin G, Kozlowski H, Kamysz W, Valensin D. Structural characterization and antimicrobial activity of the Zn(II) complex with P113 (demegen), a derivative of histatin 5. Inorg Chem. 2010; 49(19):8690–8. [PubMed: 20815365]

26. Melino S, Santone C, Di Nardo P, Sarkar B. Histatins: salivary peptides with copper(II)- and zinc(II)-binding motifs Perspectives for biomedical applications. Febs Journal. 2014; 281(3):657–672. [PubMed: 24219363]

27. Melino S, Rufini S, Sette M, Morero R, Grottesi A, Paci M, Petruzzelli R. Zn2+ Ions Selectively Induce Antimicrobial Salivary Peptide Histatin-5 To Fuse Negatively Charged Vesicles. Identification and Characterization of a Zinc-Binding Motif Present in the Functional Domain. Biochemistry. 1999; 38(30):9626–9633. [PubMed: 10423240]

28. Rydengard V, Andersson Nordahl E, Schmidtchen A. Zinc potentiates the antibacterial effects of histidine-rich peptides against Enterococcus faecalis. FEBS J. 2006; 273(11):2399–406. [PubMed: 16704414]

29. Cabras T, Patamia M, Melino S, Inzitari R, Messana I, Castagnola M, Petruzzelli R. Pro-oxidant activity of histatin 5 related Cu(II)-model peptide probed by mass spectrometry. Biochem Biophys Res Commun. 2007; 358(1):277–84. [PubMed: 17482573]

30. Houghton EA, Nicholas KM. In vitro reactive oxygen species production by histatins and copper(I,II). J Biol Inorg Chem. 2009; 14(2):243–51. [PubMed: 18975018]

31. Tay WM, Hanafy AI, Angerhofer A, Ming LJ. A plausible role of salivary copper in antimicrobial activity of histatin-5-Metal binding and oxidative activity of its copper complex. Bioorg. Med. Chem. Lett. 2009; 19(23):6709–6712. [PubMed: 19846304]

32. Cobine PA, Ojeda LD, Rigby KM, Winge DR. Yeast contain a non-proteinaceous pool of copper in the mitochondrial matrix. J Biol Chem. 2004; 279(14):14447–55. [PubMed: 14729672]

33. Rozga M, Sokolowska M, Protas AM, Bal W. Human serum albumin coordinates Cu(II) at its N-terminal binding site with 1 pM affinity. J Biol Inorg Chem. 2007; 12(6):913–8. [PubMed: 17516096]

34. Kolozsi A, Jancso A, Nagy NV, Gajda T. N-terminal fragment of the anti-angiogenic human endostatin binds copper(II) with very high affinity. J Inorg Biochem. 2009; 103(7):940–7. [PubMed: 19447499]

35. Bal W, Jeżowska-Bojczuk M, Kasprzak KS. Binding of Nickel(II) and Copper(II) to the N-Terminal Sequence of Human Protamine HP2. Chemical Research in Toxicology. 1997; 10(8): 906–914. [PubMed: 9282840]
36. Harford C, Sarkar B. Amino Terminal Cu(II)- and Ni(II)-Binding (ATCUN) Motif of Proteins and Peptides: Metal Binding, DNA Cleavage, and Other Properties. Acc. Chem. Res. 1997; 30(3):123–130.
37. Xiao Z, Wedd AG. The challenges of determining metal-protein affinities. Nat Prod Rep. 2010; 27(5):768–89. [PubMed: 20379570]
38. Kau LS, Spira-Solomon DJ, Penner-Hahn JE, Hodgson KO, Solomon EI. X-ray absorption edge determination of the oxidation state and coordination number of copper. Application to the type 3 site in Rhus vernicifera laccase and its reaction with oxygen. J. Am. Chem. Soc. 1987; 109(21): 6433–6442.
39. Pushie MJ, Shaw K, Franz KJ, Shearer J, Haas KL. Model Peptide Studies Reveal a Mixed Histidine-Methionine Cu(I) Binding Site at the N-Terminus of Human Copper Transporter 1. Inorg Chem. 2015; 54(17):8544–51. [PubMed: 26258435]
40. Shearer J, Szalai VA. The Amyloid-β Peptide of Alzheimer's Disease Binds CuI in a Linear Bis-His Coordination Environment: Insight into a Possible Neuroprotective Mechanism for the Amyloid-β Peptide. J. Am. Chem. Soc. 2008; 130(52):17826–17835. [PubMed: 19035781]
41. Rolfe MD, Rice CJ, Lucchini S, Pin C, Thompson A, Cameron AD, Alston M, Stringer MF, Betts RP, Baranyi J, Peck MW, Hinton JC. Lag phase is a distinct growth phase that prepares bacteria for exponential growth and involves transient metal accumulation. J Bacteriol. 2012; 194(3):686–701. [PubMed: 22139505]
42. Xiao Z, Loughlin F, George GN, Howlett GJ, Wedd AG. C-Terminal Domain of the Membrane Copper Transporter Ctr1 from Saccharomyces cerevisiae Binds Four Cu(I) Ions as a Cuprous-Thiolate Polynuclear Cluster: Sub-femtomolar Cu(I) Affinity of Three Proteins Involved in Copper Trafficking. J. Am. Chem. Soc. 2004; 126(10):3081–3090. [PubMed: 15012137]
43. Faller P, Hureau C, Dorlet P, Hellwig P, Coppel Y, Collin F, Alies B. Methods and techniques to study the bioinorganic chemistry of metal–peptide complexes linked to neurodegenerative diseases. Coord. Chem. Rev. 2012; 256(19–20):2381–2396.
44. Sokolowska M, Bal W. Cu(II) complexation by "non-coordinating" N-2-hydroxyethylpiperazine-N'-2-ethanesulfonic acid (HEPES buffer). J Inorg Biochem. 2005; 99(8):1653–60. [PubMed: 15993944]
45. Schwab S, Shearer J, Conklin SE, Alies B, Haas KL. Sequence proximity between Cu(II) and Cu(I) binding sites of human copper transporter 1 model peptides defines reactivity with ascorbate and O. J Inorg Biochem. 2015
46. Kim BE, Nevitt T, Thiele DJ. Mechanisms for copper acquisition, distribution and regulation. Nat Chem Biol. 2008; 4(3):176–85. [PubMed: 18277979]
47. Nevitt T, Ohrvik H, Thiele DJ. Charting the travels of copper in eukaryotes from yeast to mammals. Biochim Biophys Acta. 2012; 1823(9):1580–93. [PubMed: 22387373]
48. Samanovic MI, Ding C, Thiele DJ, Darwin KH. Copper in microbial pathogenesis: meddling with the metal. Cell Host Microbe. 2012; 11(2):106–15. [PubMed: 22341460]
49. Downie JA, Garland PB. An antimycin A- and cyanide-resistant variant of Candida utilis arising during copper-limited growth. Biochem. J. 1973; 134(4):1051–1061. [PubMed: 4357711]
50. Wohlrab H, Jacobs EE. Copper-deficient mitochondria electron transport and oxidative phosphorylation. Biochemical and Biophysical Research Communications. 1967; 28(6):998–1002. [PubMed: 6064601]
51. Wohlrab H, Jacobs EE. Copper-deficient mitochondria spectrophotometric determination of cytochromes. Biochemical and Biophysical Research Communications. 1967; 28(6):991–997. [PubMed: 6064600]
52. Helmerhorst EJ, Breeuwer P, van't Hof W, Walgreen-Weterings E, Oomen L, Veerman ECI, Amerongen AVN, Abee T. The cellular target of histatin 5 on Candida albicans is the energized mitochondrion. J. Biol. Chem. 1999; 274(11):7286–7291. [PubMed: 10066791]

53. Tati S, Li R, Puri S, Kumar R, Davidow P, Edgerton M. Histatin 5-spermidine conjugates have enhanced fungicidal activity and efficacy as a topical therapeutic for oral candidiasis. Antimicrob Agents Chemother. 2014; 58(2):756–66. [PubMed: 24247141]
54. Oppenheim FG, Helmerhorst EJ, Lendenmann U, Offner GD. Anti-candidal activity of genetically engineered histatin variants with multiple functional domains. PLoS One. 2012; 7(12):e51479. [PubMed: 23251551]
55. Oudhoff MJ, Kroeze KL, Nazmi K, van den Keijbus PA, van 't Hof W, Fernandez-Borja M, Hordijk PL, Gibbs S, Bolscher JG, Veerman EC. Structure-activity analysis of histatin, a potent wound healing peptide from human saliva: cyclization of histatin potentiates molar activity 1,000-fold. FASEB J. 2009; 23(11):3928–35. [PubMed: 19652025]
56. Jang WS, Li XS, Sun JN, Edgerton M. The P-113 fragment of histatin 5 requires a specific peptide sequence for intracellular translocation in Candida albicans, which is independent of cell wall binding. Antimicrob Agents Chemother. 2008; 52(2):497–504. [PubMed: 17999963]
57. Giacometti A, Cirioni O, Kamysz W, D'Amato G, Silvestri C, Del Prete MS, Licci A, Riva A, Lukasiak J, Scalise G. In vitro activity of the histatin derivative P-113 against multidrug-resistant pathogens responsible for pneumonia in immunocompromised patients. Antimicrob Agents Chemother. 2005; 49(3):1249–52. [PubMed: 15728942]
58. Ruissen ALA, Groenink J, Van ’t Hof W, Walgreen-Weterings E, van Marle J, van Veen HA, Voorhout WF, Veerman ECI, Nieuw Amerongen AV. Histatin 5 and derivatives: Their localization and effects on the ultra-structural level. Peptides. 2002; 23(8):1391–1399. [PubMed: 12182939]
59. Ruissen AL, Groenink J, Helmerhorst EJ, Walgreen-Weterings E, Van't Hof W, Veerman EC, Nieuw Amerongen AV. Effects of histatin 5 and derived peptides on Candida albicans. Biochem. J. 2001; 356(Pt 2):361–368. [PubMed: 11368762]
60. Himes RA, Park GY, Barry AN, Blackburn NJ, Karlin KD. Synthesis and X-ray Absorption Spectroscopy Structural Studies of Cu(I) Complexes of HistidylHistidine Peptides: The Predominance of Linear 2-Coordinate Geometry. J. Am. Chem. Soc. 2007; 129(17):5352–5353. [PubMed: 17411054]
61. Edelhoch H. Spectroscopic Determination of Tryptophan and Tyrosine in Proteins*. Biochemistry. 1967; 6(7):1948–1954. [PubMed: 6049437]
62. Gill SC, von Hippel PH. Calculation of protein extinction coefficients from amino acid sequence data. Anal. Biochem. 1989; 182(2):319–326. [PubMed: 2610349]
63. Brenner AJ, Harris ED. A Quantitative Test for Copper Using Bicinchoninic Acid. Anal. Biochem. 1995; 226(1):80–84. [PubMed: 7785783]
64. GraphPad Prism. 7 www.graphpad.com.
65. Martell, AE., Smith, RM. Critical Stability Constants. Vol. 5. Plenum Press; New York: 1982.
66. Kundra SK, Katyal M, Singh RP. Spectrophotometric determination of copper(I) and cobalt(II) with ferrozine. Anal. Chem. 1974; 46(11):1605–1606.
67. George, GN., Pickering, IJ. EXAFSPAK. 2001. http://www-ssrl.slac.stanford.edu/exafspak.html
68. Ankudinov AL, Rehr JJ. Relativistic calculations of spin-dependent x-ray-absorption spectra. Physical Review B. 1997; 56(4):R1712–R1716.
69. Lieberman RL, Kondapalli KC, Shrestha DB, Hakemian AS, Smith SM, Telser J, Kuzelka J, Gupta R, Borovik AS, Lippard SJ, Hoffman BM, Rosenzweig AC, Stemmler TL. Characterization of the Particulate Methane Monooxygenase Metal Centers in Multiple Redox States by X-ray Absorption Spectroscopy. Inorg. Chem. 2006; 45(20):8372–8381. [PubMed: 16999437]

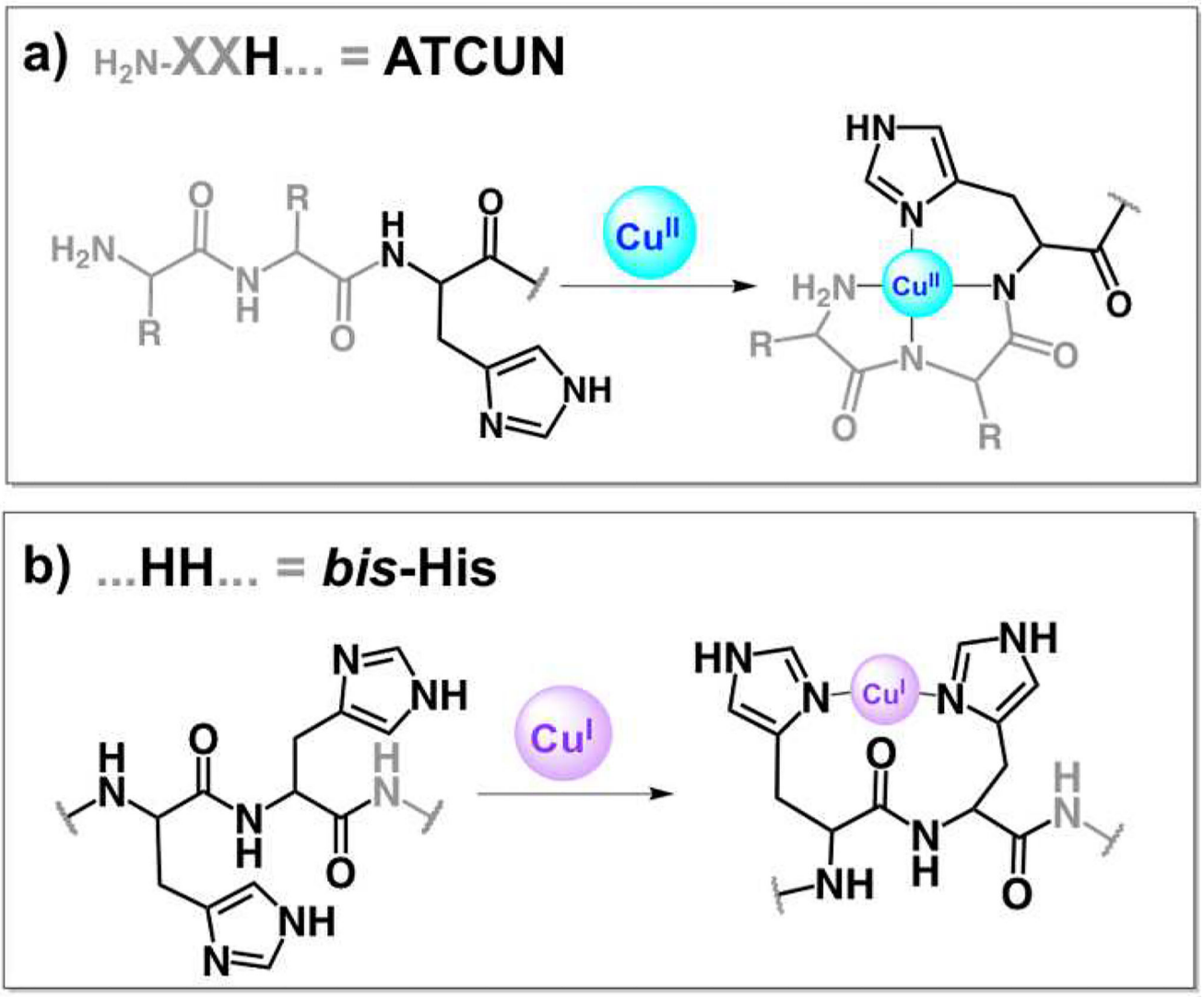

Figure 1.

Signature Cu-binding motifs present in histatin peptides: **a)** a free amino terminus and a histidine in the third position make ATCUN motifs (**a**mino-terminal **Cu**/**N**i binder) favorable for square planar Cu(II); **b)** adjacent histidines (*bis*-His) anchor Cu(I) in a linear fashion, but can accommodate higher coordination if additional ligands contribute (only linear shown).

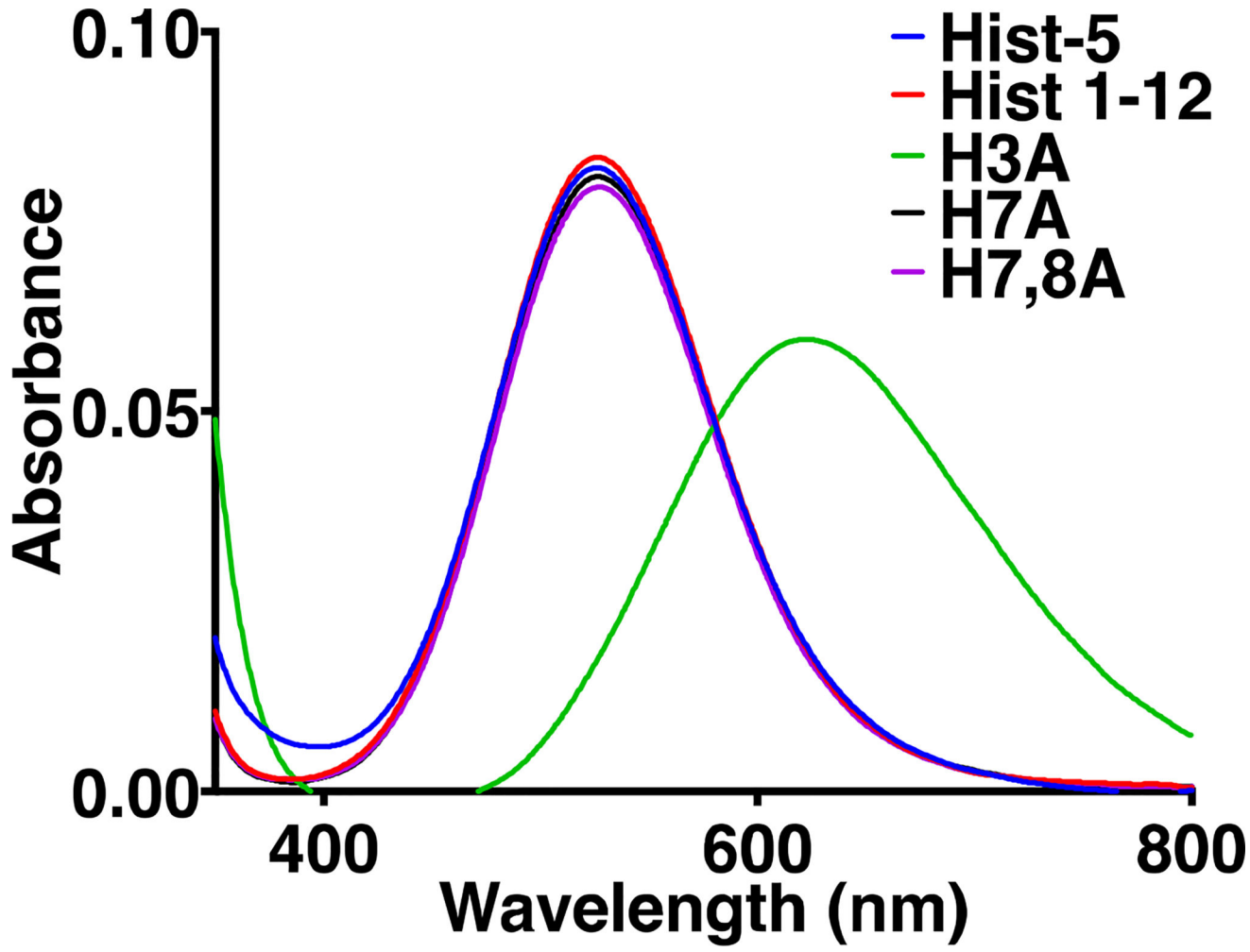

Figure 2. Absorption spectra of Cu(II)-peptides

Absorption spectra for Hist-5 and model peptides (1 mM) with 0.8 equiv. of $CuSO_4$ in 50 mM HEPES buffer, pH 7.4. The absorbance feature at 530 nm (ε = 110 $M^{-1}cm^{-1}$) is characteristic of a Cu(II)-bound ATCUN site. Replacement of the third His abolishes the ATCUN site, hence the absorbance red-shift to ~620 nm for peptide H3A.

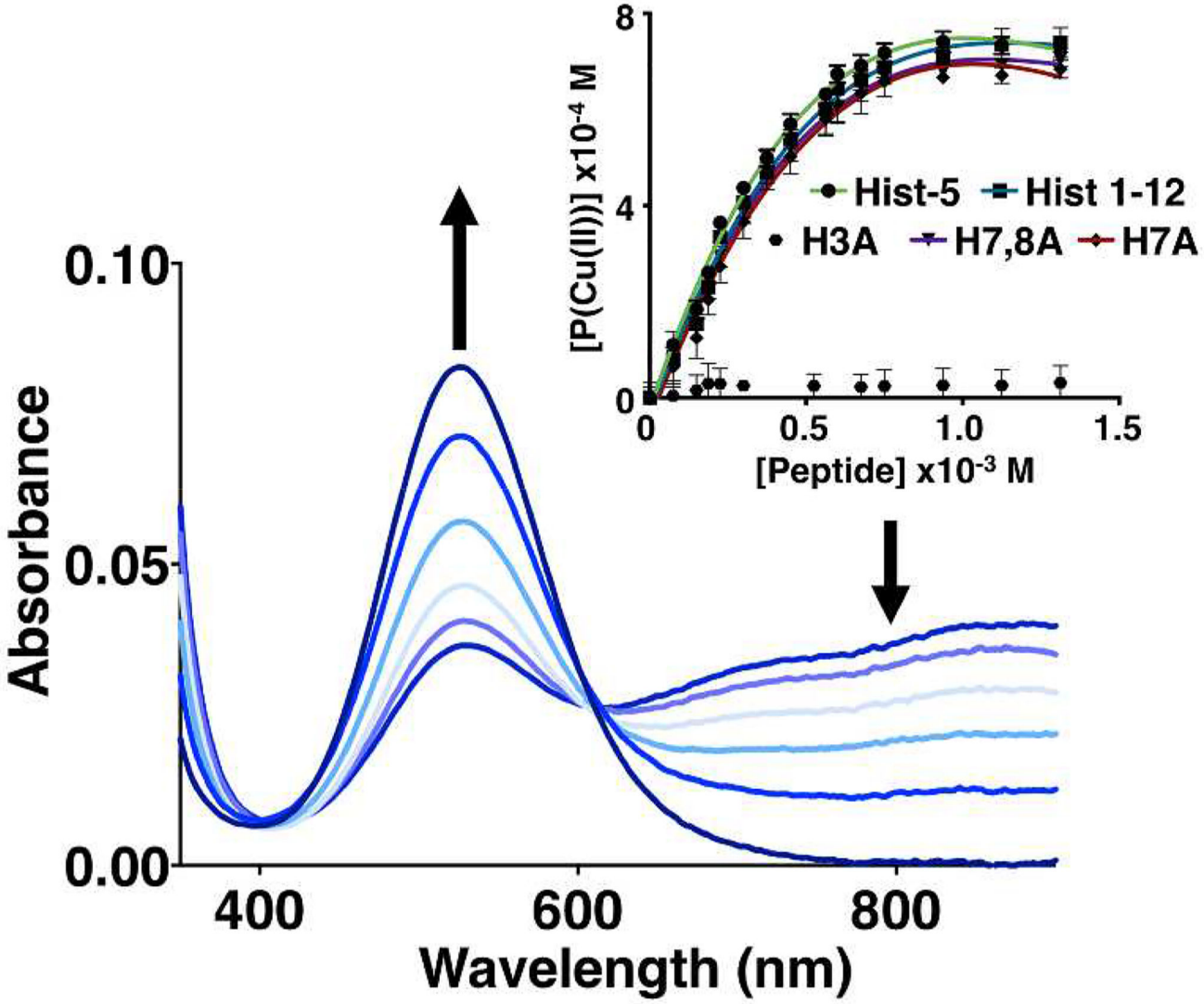

Figure 3. Cu(II) binding competition with NTA as a competitive chelator

Optical titration of up to 2 equiv of Hist-5 into a 0.8 mM solution of 1:1 NTA:Cu(II) in 50 mM HEPES buffer, pH 7.4. [Inset]: Comparison of titration data from all peptides, showing increase of the Cu-Peptide complex (taken from $Abs_{850\ nm}$ decrease) as a function of added peptide. All of the peptides compete effectively with NTA for Cu(II), with the exception of H3A, the only sequence lacking an ATCUN motif. Lines represent the best fit to Eq. 2 and error bars represent the standard deviation from the average of triplicate measurements.

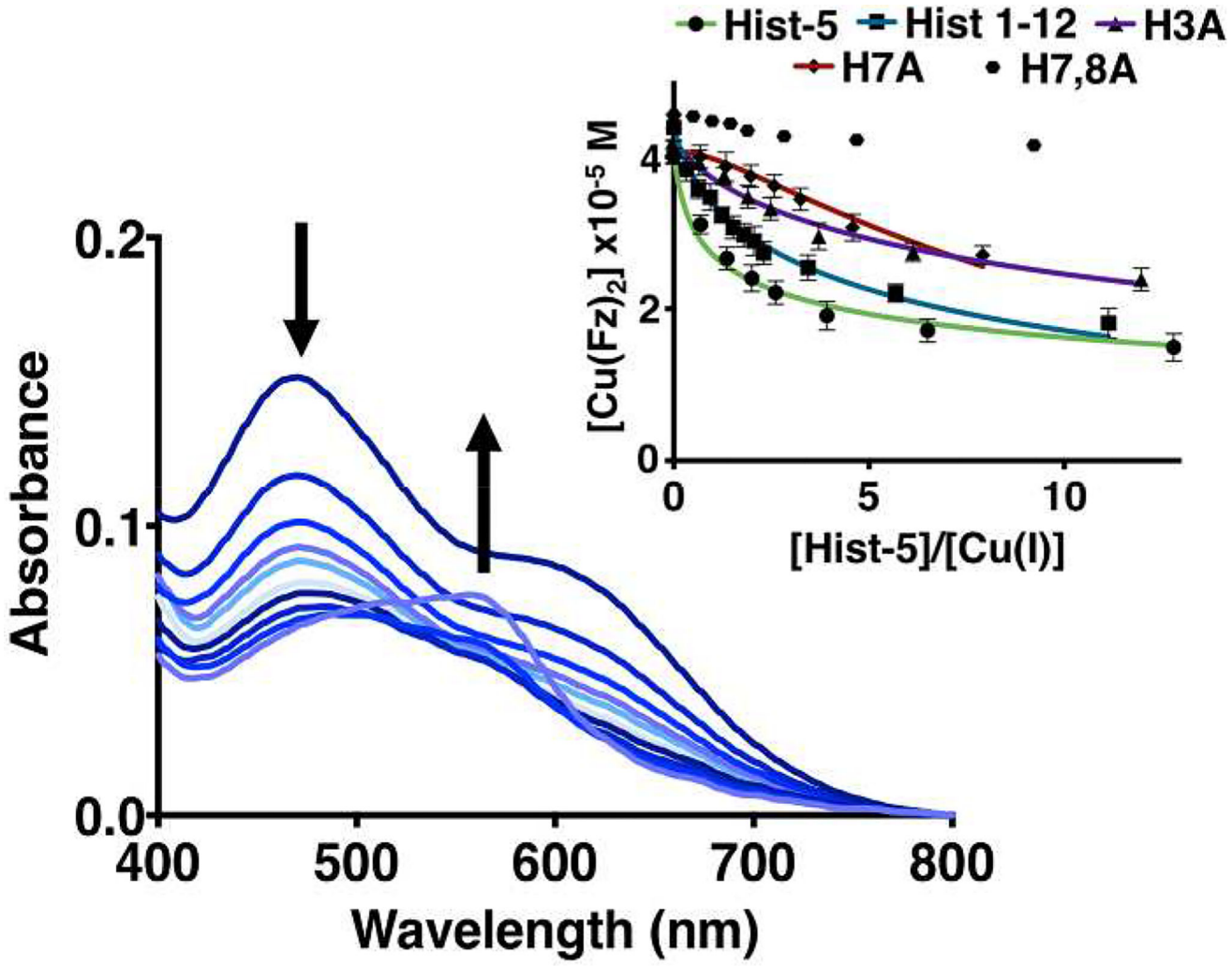

Figure 4. Cu(I) binding competition using Fz as competitive chelator

Optical titration of Hist-5 to a 55 μM solution of $[Cu(I)(Fz)_2]^{3-}$ in 50 mM HEPES buffer, pH 7.4, in anaerobic conditions. [Inset]: Comparison of the ability of all the peptides to outcompete Fz for Cu(I) binding. Error bars represent the standard deviation from the average of triplicate measurements; lines represent the best fit to the equilibrium expressed in Eqs. 7 and 8 (see experimental section).

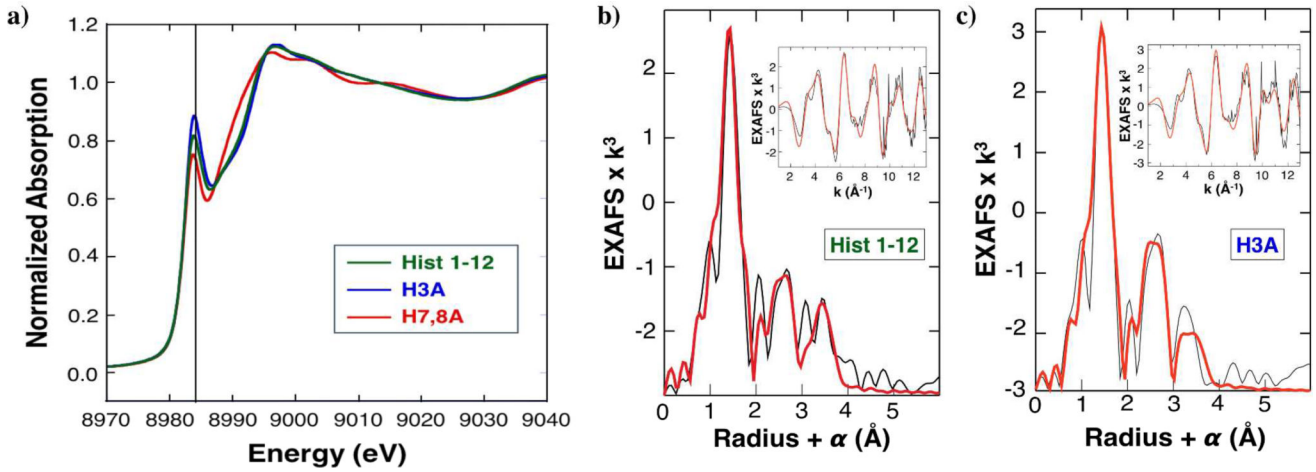

Figure 5. X-ray absorption spectroscopy data for Hist 1–12, H3A, and H7,8A

a) XANES spectra for Hist 1–12 (green), H3A (blue), and H7,8A (red). The vertical line is 8984 eV. EXAFS spectra for **b)** Hist 1–12 and **c)** H3A (k^3 weighted) in k space ($Å^{-1}$) and the corresponding Fourier transform of the data (Å, offset by phase shift α). Unfiltered and unsmoothed data are the thin line in each frame; the thick line represents the best 5 and 4 shell fit to the data (for Hist 1–12 and H3A respectively, as shown in bold in Table S1). Data were fit over a k-range of 1–13 $Å^{-1}$.

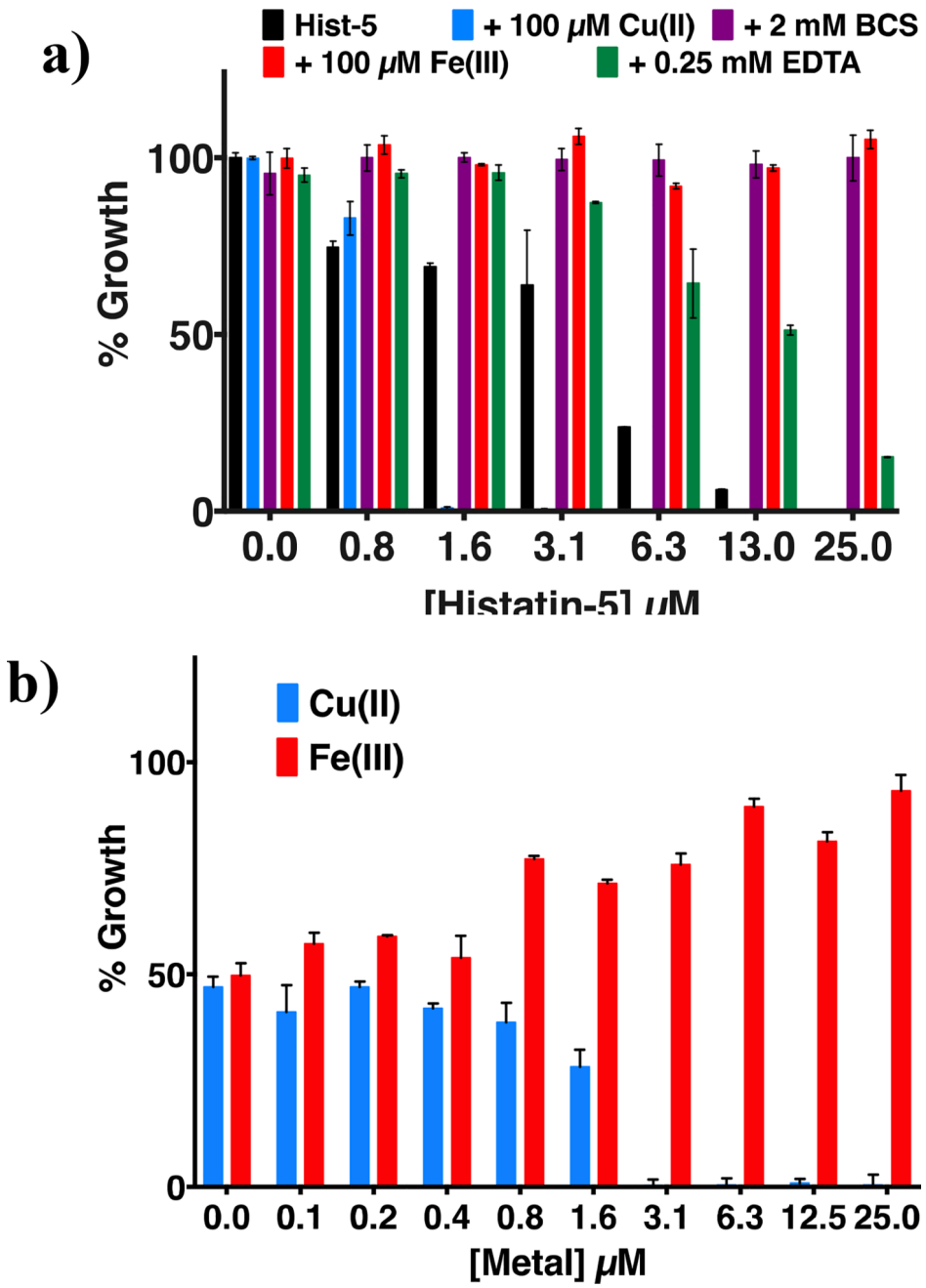

Figure 6. Antifungal susceptibility assay of *C. albicans* against Hist-5 in metal-supplemented and depleted growth conditions

Growth inhibition, as measured by OD_{600} readings after 48 h in YPD medium at 30 °C of *C. albicans* that had been previously exposed for 1.5 h to: **a)** increasing concentrations of Hist-5 alone or in combination with $CuSO_4$, $FeCl_3$, BCS, or EDTA at indicated concentrations. Supplemental Cu enhanced the antifungal activity of Hist-5, whereas Fe(III) and metal chelators (BCS, EDTA) decreased it. **b)** Contrasting effects of supplemental Cu(II) and Fe(III) on *C. albicans* % Growth upon 6.2 μM Hist-5 treatment are apparent at low μM concentrations.

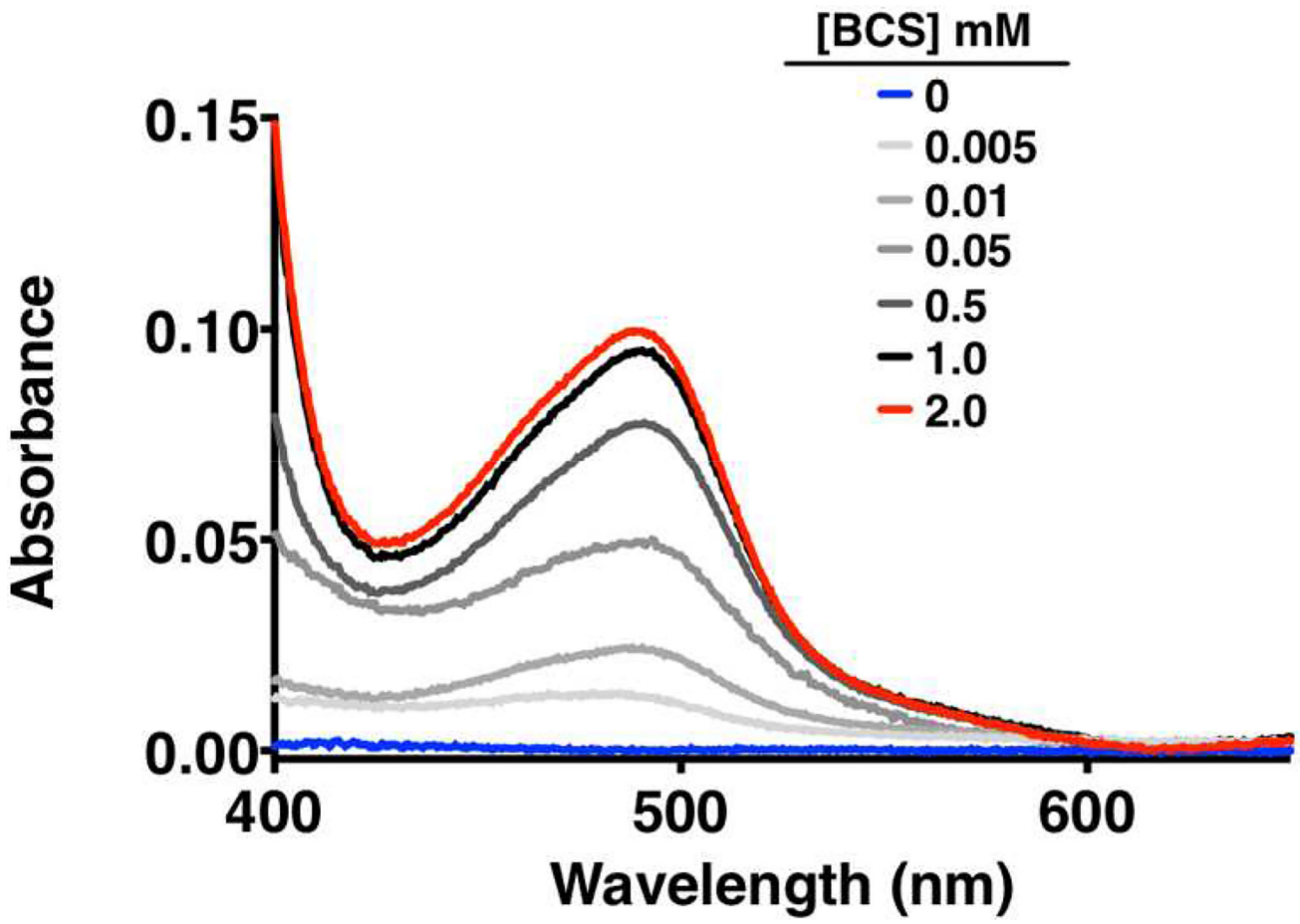

Figure 7. The Cu chelator BCS is capable of outcompeting Hist-5 for Cu binding

UV-visible spectra of 7.0 μM Hist-5 and 7.0 μM Cu(II)SO_4 in YPD media incubated for an 1 h with increasing concentration of BCS from 0 to 2 mM.

a)

Overnight YPD Culture Condition	Co-treatment Condition	Cell-associated Cu Content (nmol Cu/mg P)
I) -	-	1.0 ± 0.4
II) -	2 mM BCS	0.8 ± 0.4
III) 2 mM BCS	-	0.308 ± 0.006
IV) 100 μM Cu(II)	-	126 ± 7

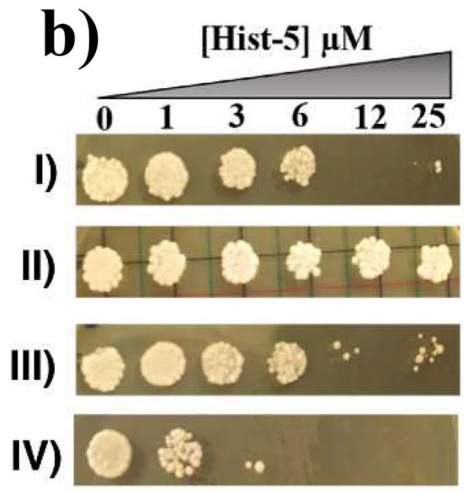

Figure 8.

a) ICP-MS reveals cell-associated Cu content of *C. albicans* cells grown under indicated conditions; b) Killing assay (spot test) under growth and treatment conditions as indicated in (a): I) Yeast cells exposed to 12 µM and higher Hist-5 following the normal protocol failed to grow. II) Cells exposed to Hist-5 in combination with 2 mM BCS recovered growth at all concentrations of Hist-5 tested. III) Cells grown overnight in YPD with 2 mM BCS then washed prior to Hist-5 exposure were not as susceptible to concentrations above 12 µM of Hist-5 as cells grown in YPD. In contrast, IV) cells grown overnight in YPD + 100 µM $CuSO_4$ prior to Hist-5 treatment were sensitized to Hist-5.

Table 1

Names, sequences, and apparent Cu-binding affinities (50 mM HEPES, pH 7.4) of Hist-5 and truncated peptides.[a]

Peptide	Sequence	log *K* Cu(II)	log (K_1) Cu(I)	log (K_2) Cu(I)	Model [P:Cu(I)]
Hist-5	DS**H**^{3}AKR**H**^{7}**H**^{8}GYKRKF**H**EK**H**^{18}**H**^{19}S**H**RGY	11.1 ± 0.2	7.8 ± 0.2	7.6 ± 0.3	1:2
Hist 1-12	DS**H**^{3}AKR**H**^{7}**H**^{8}GYKR	11.4 ± 0.4	7.1 ± 0.3	-	1:1
H3A	DS**A**^{3}AKR**H**^{7}**H**^{8}GYKR	N/A	6.7 ± 0.4	-	1:1
H7A	DS**H**^{3}AKR**A**^{7}**H**^{8}GYKR	11 ± 1	5.1 ± 0.1[b]	-	2:1
H7,8A	DS**H**^{3}AKR**A**^{7}**A**^{8}GYKR	11.6 ± 0.6	N/A	N/A	N/A

[a] Histidines (H) are bolded, alanine (A) substitutions are bolded in red, and both A and H of interest are labelled with the number of their location in the peptide sequence. Both ATCUN and *bis*-His motifs are underlined. All peptides contain a free amino N-terminus. The C-terminus is a carboxylic acid for Hist-5, and an amide for the truncations. Apparent affinity constants (log K) for Cu(II) and Cu(I) were determined in 50 mM HEPES buffer, pH 7.4, according to the indicated stoichiometric model.

[b] H7A binds in a 2:1 fashion (peptide:Cu(I)), therefore two peptide binding events occur for the formation of the complex, giving an overall log β_2 of 10.1

Table 2

EC_{50} values for Hist-5, full-length mutants, and truncated peptides against yeast morphotype of *C. albicans* under metal supplemented and depleted conditions

Peptide sequences are shown in Table 1; His-to-Ala replacements of full-length Hist-5 follows the numbering in Table 1.

Peptide	EC_{50} (μM)				
	No Supplement	+ 100 μM $Cu(II)SO_4$	+ 2 mM BCS	+ 100 μM $Fe(III)Cl_3$	+ 0.25 mM EDTA
Hist-5	5.15 ± 0.03	1.36 ± 0.02	>100	>100	22.5 ± 0.1
Hist-5(H3A)	15.8 ± 0.04	5.00 ± 0.01	>100	>100	>100
Hist-5(H7,8A)	>100	>100	>100	>100	>100
Hist-5(H18,19A)	13.0 ± 0.01	1.35 ± 0.09	>100	>100	>100
Hist 1–12	>25	4.74 ± 0.02	>100	>100	>100
H3A	>25	6.16 ± 0.04	>100	>100	>100
H7A	>25	14.06 ± 0.05	>100	>100	>100
H7,8A	>25	>25	>100	>100	>100